A STUDY ON MECHANICAL CHARACTERISTICS OF LITHIUM-POLYMER POUCH CELL BATTERY FOR ELECTRIC VEHICLE

Hyung Yun Choi
HongIk University, Mechanical System Design Engineering Department
Korea, Republic of
Inhyeok Lee
Hankook ESI
Korea, Republic of
June Soo Lee, Young Man Kim, Hyunjin Kim
SK Innovation
Korea, Republic of
Paper Number 13-0115

ABSTRACT

In order to characterize deformation and failure behaviors of Lithium-Polymer pouch cell battery and its components, various mechanical tests were performed. Uniaxial tensile properties of electrodes, separator, and pouch cover were obtained from coupon tests. Effects of temperature and strain rate on the mechanical behavior were also investigated. The three-point bending tests with and without pouch vacuum were performed to quantify the stiffening effect due to the pouching vacuum as well as quantifying the bending rigidity and failure load of the pouch cell. Static and dynamic pin drop tests were also carried out to investigate the failure mode and impact energy threshold for the perforation. The vibration responses, i.e., natural frequencies of pouch cell were obtained from impact hammer and shaker excitation tests. A finite element model of pouch cell using shell and membrane elements was also constructed. The same number of stacking layers in separator/electrode assembly was represented in the model. The solid state electrolyte that occupies very tiny volume between layers in the pouch was modeled by tied option of which the normal and shear moduli were calibrated from the three-point bending simulation.

INTRODUCTION

The Lithium-Polymer battery is widely adopted RESS (Rechargeable Energy Storage System) in electric vehicle and becomes a key component especially considering the safety issue. The pouch cell, a common design of Lithium battery is in a vacuum packed thin plate shape in which many stacking layers of thin cathode and anode electrodes are alternately winded by a long ribbon of polyolefin separator. This separator/electrode assembly including widespread solid-state electrolyte between each layer are sealed inside a flexible thin plastic/aluminum pouch cover. Multiple cells are assembled to a module level and several modules are further joined together into a battery pack in various shapes to be installed at the safest position in electric vehicle, e.g., in a tray shape under floor or in a fuel tank shape behind the rear seat.

Sahraei et al [1] reported their effort on a FE modeling of pouched Lithium ion cell. Their model predicted force-displacement relations for bending, axial and through thickness compressions, and also onset of short circuit during a punch loading. However the outcome of the model simulation is rather limited to the overall behavior of the pouch cell than local stress and strain level because their model was built with lumped solid and shell elements to model layers of electrodes, separator, and electrolyte altogether.

In this study, comprehensive mechanical tests were performed to characterize deformation and failure behavior of Lithium-Polymer pouch cell and its components. Effects of temperature, strain rate, and anisotropy on the mechanical behavior were also investigated. Vibration characteristics were examined by impact hammer and shaker excitation tests to secure in situ natural frequencies and associated mode shape of the pouch cell. In addition, there was an effort to build a detailed finite element model of LB pouch cell in this study. Precise geometry of pouch cell and its components to the level of single layers of separator and electrode were reconstructed. A unique modeling approach was employed to represent the mechanical behaviors of solid-state electrolyte which needs an extra numerical treatment due to its very thin and complicated mechanical properties. Using this FE model of pouch cell, virtual simulation of mechanical deformation and failure of pouch cell is attempted in both component and assembly levels to validate against test results.

CHARACTERIZATION OF MECHANICAL BEHAVIOR

In this study, used but serviceable Lithium Polymer pouch cells of 10Ah capacity designed for a serial hybrid vehicle were procured for various mechanical

tests. In order to avoid possible electric short circuit during tests, all cells were completely discharged and further disassembled into components, i.e., electrodes and separators for the coupon test. The stained solid-state polymer electrolyte on electrodes and separator layers was totally washed out using ethylene carbonate solution but the coating layers on electrodes were preserved as undamaged. Then they were hung up to dry in a hood with ventilation system. Table 1 lists mechanical tests performed to characterize deformation and failure behaviors of Lithium polymer pouch cell battery at each individual component level as well as at integrated pouch cell unit.

Table 1 List of tests to characterize mechanical behaviors of Lithium Polymer pouch cell battery

Test	Specimen	Test parameters	Objective
Tension	Coupons of Electrodes, separator, pouch cover	Temperature, Strain rate, anisotropy	Basic tensile properties of each component
Bending	Pouch cell unit	Temperature, Strain rate, vacuum	Flexural stiffness and strength
Quasi static pin penetration	Electrodes, separator, pouch cover	Temperature(3), Strain rate(2)	Failure threshold of each component
Drop impact penetration	Pouch cell unit	Drop height	Failure threshold
Impact Hammer	Pouch cell unit	-	Modal frequency
Shaker excitation	Pouch cell unit	Excitation direction, Boundary condition	Vibration response

Tension test

Uniaxial tension test was performed to characterize basic tensile properties of each component in Lithium Polymer pouch cell battery. The temperature standard in ASTM E8M-09 was adopted using an environment chamber with 1kN load cell and visual extensometer (Instron UTM 5569). Test coupon was cut into a dumbbell shape in a size of total length of 120mm, grip width of 25mm, gauge length of 40mm, and gauge width of 10mm as specified in KS-M3054. There were three test parameters, i.e., temperature (-40℃, 22℃, 65℃), strain rate (1mm/min, 50mm/min for electrodes, 490mm/min for separator and pouch cover), and loading direction (anisotropy, 0˚, 45˚, 90˚). Tensile test with each condition was repeated for three times to obtain mean and standard deviation values of elastic modulus, yield strength, tangent modulus, failure strength, and failure strain of each component. Some of representative stress-strain curves are introduced in Figures. 1-6.

Figure 1 shows representative engineering stress-strain relations of all components at room temperature (22℃), lower strain rate (1 mm/min), and longitudinal direction (0˚). The initial elastic moduli of two electrodes, cathode (Al) and anode (Cu) were similar to each other. However cathode specimen showed higher yield and failure strengths but lower failure strain than anode did. The separator exhibited the lowest modulus but highest failure strain.

Two electrodes, cathode and anode showed temperature and strain rate dependencies as in Figures. 2 and 3. However there was no noticeable anisotropy found from the tensile response of electrodes. Both electrodes exhibited increasing failure strength and decreasing failure strain at lower temperature as shown in Figure 2. The maximum applicable strain rate to electrodes in our test was 50mm/min (c.f., 490mm/min for separator and pouch cover) due to the measurement limit of the visual extensometer and the brittle behavior of electrodes, especially at a low temperature. It was found that there was a large variation in the measured failure strain at the higher strain rate and thus became to be hard to conclude any strain rate effect on electrodes.

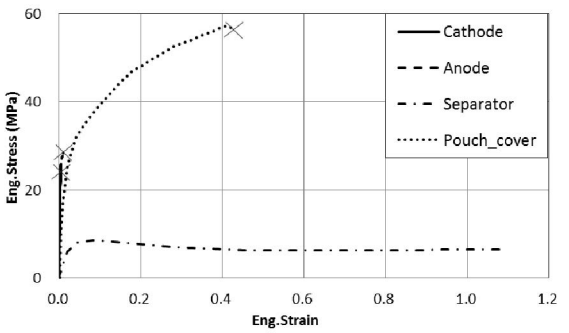

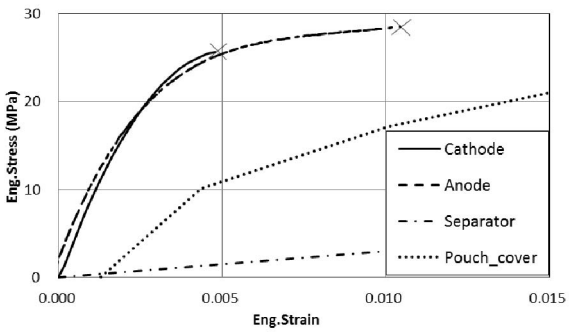

Figure 1. Normalized engineering stress-strain curves of electrodes, separator, and pouch cover (top) and zoomed initial portion (bottom) (temperature: 22℃, strain rate: 1mm/min, anisotropy: 0˚)

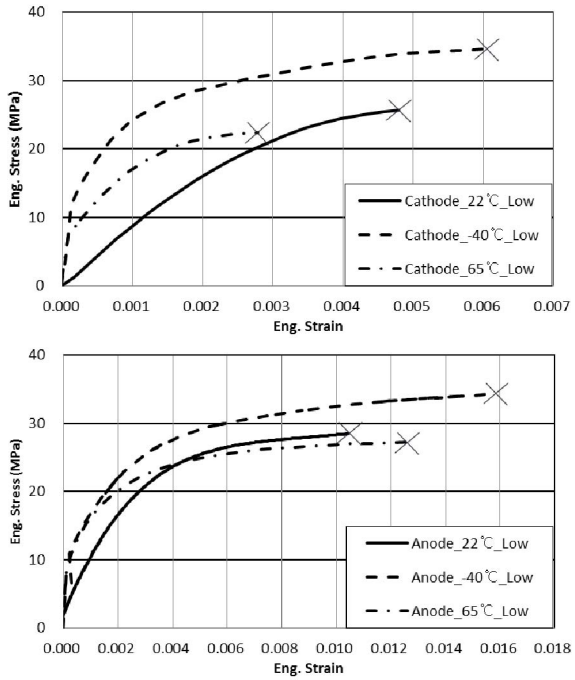

Figure 2. Temperature effect on tensile stress-strain relationship of electrodes, cathode (top) and anode (bottom), strain rate: 1mm/min, X: failure point

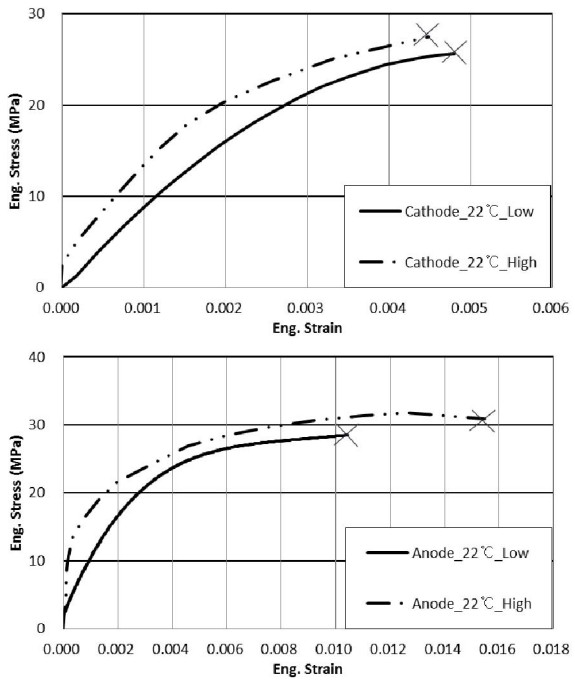

Figure 3. Strain rate effect on tensile stress-strain relationship of electrodes, cathode (top) and anode (bottom) at temperature: 22℃, Low: strain rate 1mm/min, High: strain rate 50mm/min, X: failure point

For separator and pouch cover, elastic modulus and failure strength and strain increased with the temperature as shown in Figure 4. Due to the capacity limit of the UTM machine used in this study, it was not possible to elongate the separator specimen up to the failure point at all temperature conditions.

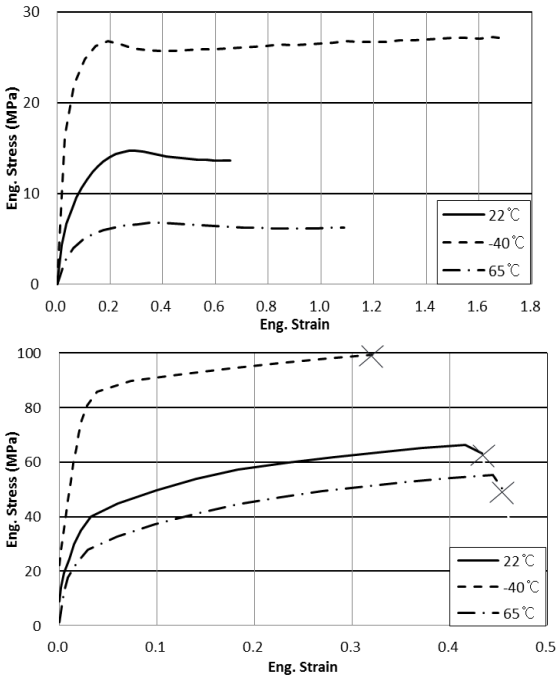

Figure 4. Temperature effect on tensile stress-strain relationship of separator (top, anisotropy: 45˚, strain rate: 1mm/min) and pouch cover (bottom, anisotropy: 0˚, strain rate: 490mm/min), X: failure point

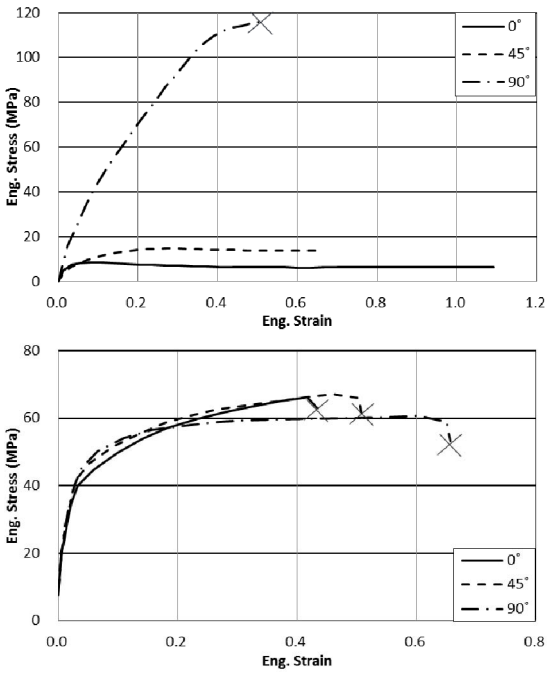

Figure 5. Anisotropy of separator (top, temperature: 22℃, strain rate: 1mm/min) and pouch cover (bottom,

temperature: 22℃, strain rate: 490mm/min)

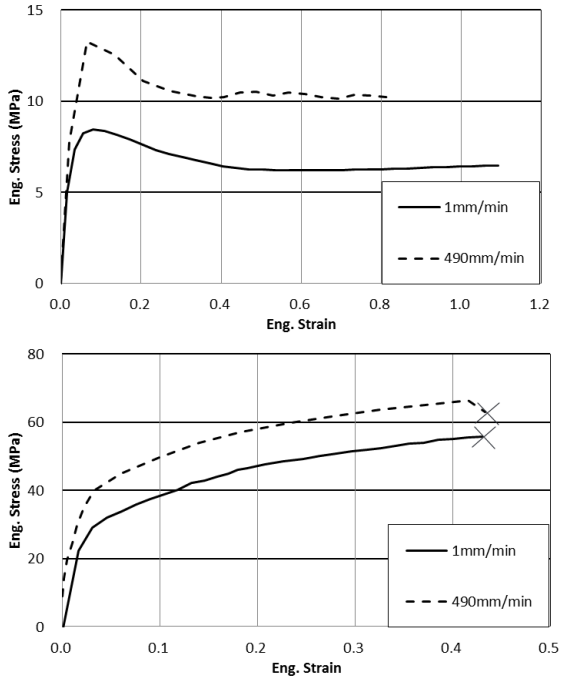

Figure 6. Strain rate effect tensile stress-strain relationship of separator (top, anisotropy: 0˚, temperature: 22˚) and pouch cover (bottom, anisotropy: 0˚, temperature: 22˚), X: failure point

Three-point bending test

Bending rigidity of the LB pouch cell depends on the degree of pouching vacuum. Also, the bonding strength between separator and electrodes is affected by the phase change of electrolyte which plays an adhesive role in a mechanical point of view. The bending stiffness and strength of the pouch cell is also largely influenced by this bonding strength. In order to characterize a bending stiffness and strength of the LB pouch cell taking the effect of pouching vacuum into consideration, three-point bending test complying KSMISO-14125 was performed. Three temperatures (-40℃, 22℃, 65℃) and two loading speeds (1mm/min, 490 mm/min) were respectively applied as test conditions. Figure 7 shows representative force-displacement relationships from three-point bending test of LB pouch cell. Both bending stiffness and strength decreased at higher temperature. Strain rate increased both bending stiffness and strength, i.e., the ultimate bending force.

Impact hammer and shaker excitation tests

Vibration characteristics of LB pouch cell were obtained from impact hammer and shaker excitation tests. A vertical impact force was applied at a corner of LB pouch cell with a free boundary condition. As shown in Figure 8, a Frequency Response Function (FRF) was acquired from the uniaxial acceleration measured at the diagonally opposite point from the same loading direction of hammer impact.

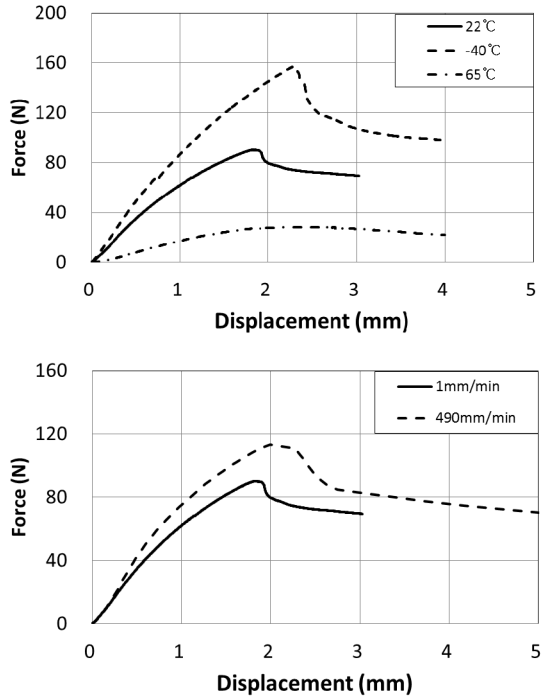

Figure 7. Force-Displacement relationship from three-point bending test of LB pouch cell; Temperature (top) and strain rate (bottom) effects

The bandwidth for natural frequency measurement in our impact hammer test was over 250 Hz and it thus became to pass beyond the range for the durability test. The durability test of battery system is usually carried out in a pack level with up to 200 Hz frequency range, which focuses on the evaluation of joining strength between lead electrode taps and separator/electrode assembly inside the cell and between cells. The main objective of the hammer impact test in our study was to identify natural frequencies of LB pouch cell as listed in Table 2.

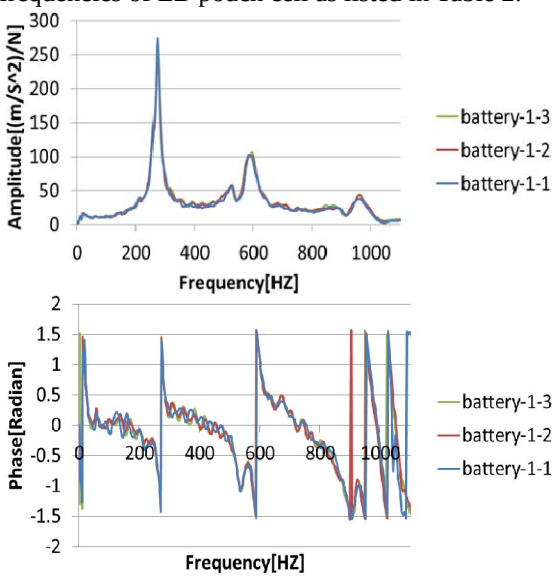

Figure 8. FRF amplitude (top) and phase of a LB pouch cell (bottom)

Table 2 Natural frequencies of LB pouch cell measured from hammer impact test

Mode	Specimen				
	#1	#2	#3	#4	Average
1st	274	284	266	244	267
2nd	-	-	-	474	474
3rd	590	602	592	-	595
4th	954	1000	945	950	962

Figure 9 is a schematic drawing of LB pouch cell describing the connection between lead electrodes and stacked layers of separator/electrodes assembly inside pouch cell by a simple elastic spring. The frequency range employed for the investment of pouch cell durability, i.e., below 200 Hz may be largely affected by this joining stiffness (i.e., spring constant in Fig. 11) between internal component (separator/electrodes assembly) and lead electrode taps and the mass of internal component. In order to characterize this dynamic property, a shaker excitation test was also performed with adopting same boundary conditions as when cells are assembled in a modular level of battery system.

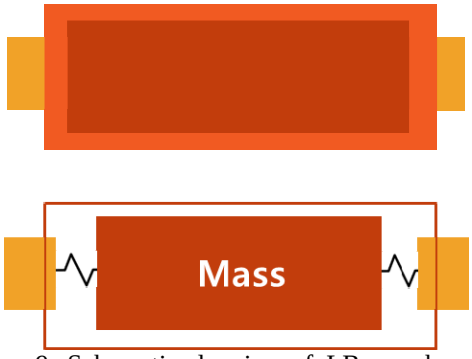

Figure 9. Schematic drawing of LB pouch cell to depict cell assembly for its dynamic response

Two kinds of clamping boundary conditions were respectively used in the shaker excitation test; 1) two edges in longitudinal directions, and 2) all four edges of pouch cell. There were three excitation directions, longitudinal (X), transverse (Y), and vertical (Z) directions, respectively. Two pouch cell specimens were used for each condition to check repeatability of the test. Figure 10(a) shows mounted control sensors which is a uniaxial accelerometer that monitors excitation signals and two triaxial accelerometers which sense vibration response output of the pouch cell specimen. The configurations of fixed boundary conditions and excitation directions of shaker test are shown in Figure 10 (b).

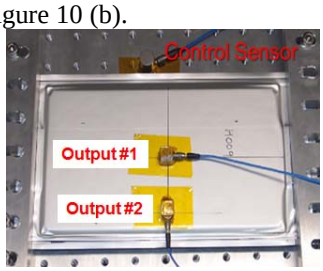

(a) Accelerometer sensors

Boundary condition	Excitation direction		
	X	Y	Z
Two-edge clamping	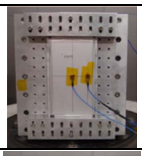	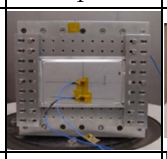	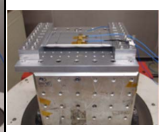
Four-edge clamping	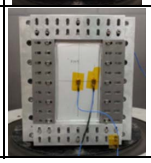	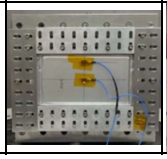	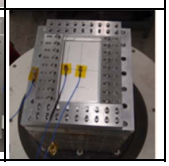

(b) Boundary conditions and excitation directions

Figure 10. Accelerometers for excitation control and output measurement and the boundary conditions and excitation directions at shaker test

Excitation frequency range was selected from 10 to 2000 Hz in sine sweep signal with 5min/sweep speed considering durability test condition and the capacity limit of the test machine (shaker: LDS, controller: B&K V875-440 LPT 600 COMBO). The magnitude of excitation was set to 1G which is one third of the required condition in the durability test. Acceleration profiles in frequency domain measured from two sensors for three excitations are shown in Figure 11. The resonant frequencies were selected where the amplitude of output signal became twice than that of input excitation amplitude. First two natural frequencies with all test conditions, i.e., two boundary conditions and three excitation directions are summarized in Table 3.

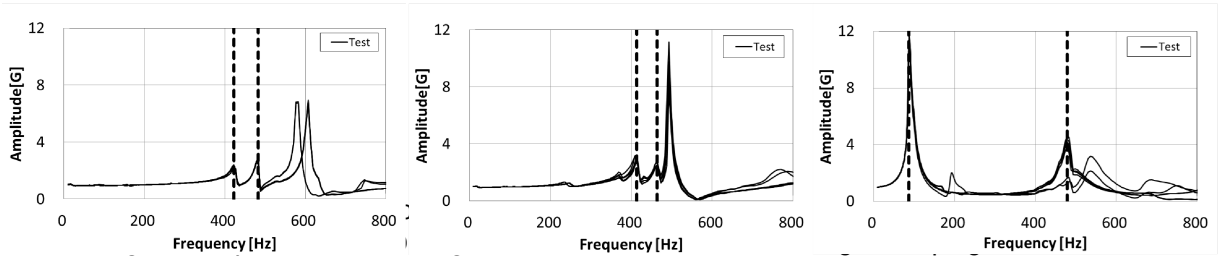

Figure 11. Acceleration response along three excitation directions with two-edge clamping boundary condition; longitudinal (left), transverse (middle), and vertical (right)

Table 3 Modal frequencies of LB pouch cell from shaker test

	Two-edge clamping			Four-edge clamping		
Mode / Excitation direction	X	Y	Z	X	Y	Z
1st (Hz)	422	414	**87**	414	422	268
2nd (Hz)	483	464	478	469	478	476

Quasi static pin penetration test

In order to characterize failure thresholds, especially in a penetration mode of LB pouch cell components, a quasi-static pin penetration test was performed. A spike shaped pin with 4.5 mm diameter was used as a penetrator on circularly clamped cell components with 45mm diameter as shown in Figure 12. Representative force-displacement curves of electrodes, separator and pouch cover are shown in Figure 13.

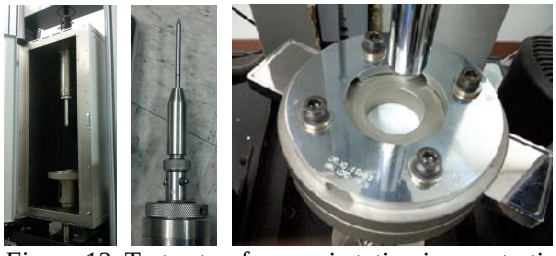

Figure 12. Test setup for quasi-static pin penetration test

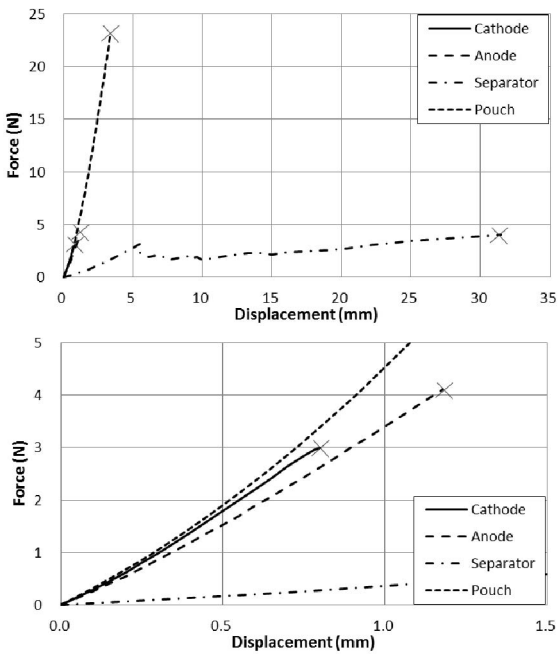

Figure 13. Force-displacement curves from quasi static pin penetration test at 22℃ (top) and zoomed initial portion (bottom)

Pin drop impact test

The characteristic of dynamic perforation of LB pouch cell was obtained from pin drop impact test (see Figure 14). Drop weight was fixed to 1.78 kg and drop height was varied from 1m to 3m high. Total ten drop impacts were performed to find out the threshold height to perforate the pouch cell. Threshold height was found to be between 1.3m and 1.4m which corresponds 22.7J and 24.4J in drop energy. Perforation shape of a pouch cell from the pin drop impact test is shown at Figure 15.

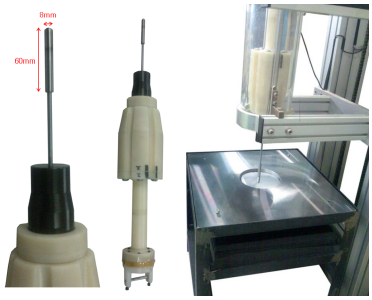

Figure 14. Test setup for drop impact on pouch cell

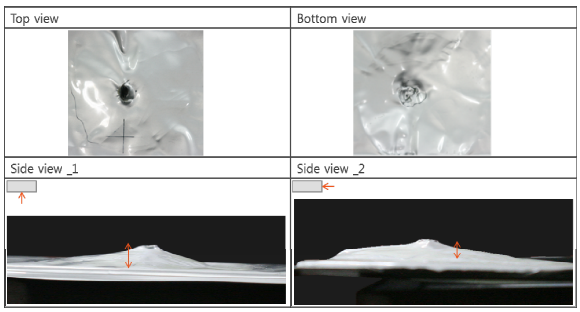

Figure 15. Perforation of pouch cell from drop impact test; impact mass 1.78 kg, impact height 1.4 m

FE MODELING OF LITHIUM-POLYMER BATTERY POUCH CELL AND ITS VALIDATION

Detailed stacking sequence and winding of separator/electrodes in LB pouch cell is shown in Figure 16. The thickness of each component was directly measured from the disassembled cell specimen except the electrolyte layer

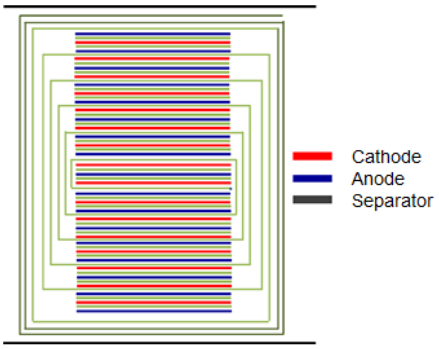

Components		No. of layers	Thickness(mm)
Cathode	Al substrate	16	0.015
	Cobalt coating	32	0.045
Anode	Cu substrate	17	0.012
	Carbon coating	34	0.041
Pouch cover		2	0.156
Separator		35	0.029
Electrolyte		69	0.005
Total		205	4.950

Figure 16. Schematic drawing and detailed thickness distributions of separator/electrode assembly in LB pouch cell

In an aspect of finite element modeling, the most unique approach of this study could be the electrode and electrolyte models in a pouch cell structure. The electrodes are made of very thin pure metal substrates (Al for cathode and Cu for anode) coated by Lithium compound (Cobalt compound for cathode and Carbon compound for anode) and their thicknesses are around 0.1mm. Each electrode layer was modeled by three stacking shell elements, i.e., middle element represented pure metal substrate and upper and lower elements for coating layers, respectively. The nodes of three layered shell elements are rigidly tied together for all degree of freedoms. The solid-state electrolyte polymer layer was only 0.005mm thick in a pouch cell and therefore the direct measurement of mechanical property and assigning a physical element in the FE pouch cell model became quite difficult. So, the layers of electrolyte were modeled by a link element (Material type #304 in Pam-Crash [4]) which connected nodal points by a penalty spring with normal and shear stiffness. The contribution of binding strength of electrolyte in separator/electrode winding assembly depends on this normal and shear stiffness which are to be determined from a three-point bending analysis. The spacing of shell elements through the thickness direction is schematically presented in Figure 17. As mentioned in the previous section, pouching vacuum plays an important role in the mechanical integrity of the pouch cell. Thus, upper and lower sides of pouch cover were rigidly tied together to numerically represent the pouching vacuum inside the cell as shown in Figure 18. Mechanical properties, such as elastic modulus, yield strength, tangent modulus, and failure strength obtained from tension tests in above section were assigned into pouch shell components. The total number of nodes and elements of finite element pouch cell model in Fig. 20 were 134,086 and 126,256, respectively.

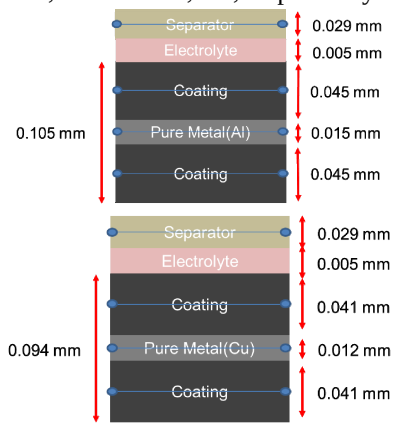

Figure 17. Spacing of shell elements through the cell thickness direction, Cathode (top) and Anode (bottom) in separator/electrode winding assembly

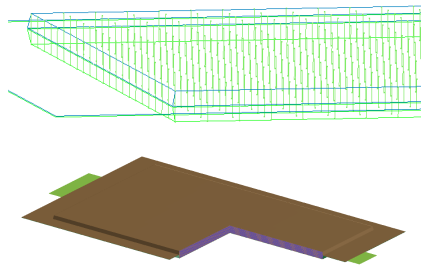

Figure 18. Tied link between upper and lower pouch cell covers to represent pouching vacuum condition (top), Lithium polymer battery finite element model with a quarter cut (bottom)

Three-point bending simulation

A three-point bending simulation was performed with unpouched separator/electrodes assembly to estimate the normal and shear stiffness of tied link which represent the thin layers electrolyte. (Figure 19 left) The stiffness of tied link was determined to match the simulated force-displacement relationship against the test measurement. Thereafter, the modeling of electrolyte was validated with two other conditions in pouch cell level, i.e., with and without pouching vacuum (Figure 19 right). The force–displacement relationships from simulation were compared with test measurements for various pouching conditions are shown in Figure 20. It is noted that one of test result of depouched cells was found to have very lower reaction force than the other two test results. The effect of pouching vacuum on the mechanical integrity of pouch cell can be seen from the Figure 21 which displays two folded center region of the cell with and without pouching vacuum conditions. It was found that the

pouch cell slightly inflated and the cover got wrinkled when the vacuum was absent. The pouching vacuum thus restrained a formation of internal vacant space, i.e., the separation of pouch cover from the internal separator/electrode assembly even at the extreme deformation of the pouch cell.

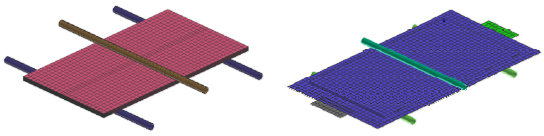

Figure 19. Finite element models for three-point bending simulation ; unpouched internal separator/electrodes assembly (left) and pouch cell unit (right)

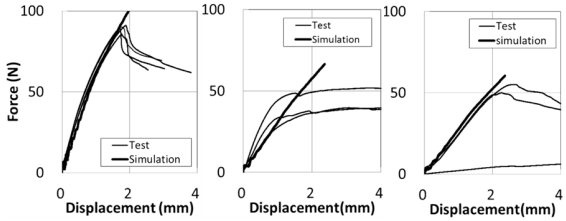

Figure 20. Comparison of test and simulation results of 3-point bending test: effects of pouching and pouching vacuum (loading speed 1mm/min at 22°C) pouched cell with vacuum (left), pouched cell without vacuum (middle), and depouched cell (right)

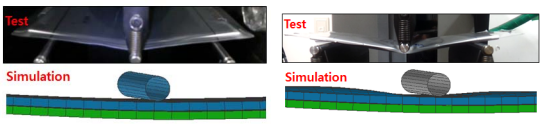

With pouch vacuum without pouch vacuum

Figure 21. Effect of pouching vacuum on bending behavior of pouch cell. Test and simulation are in the same state at peak force.

Effects of temperature and loading speed on three-point bending characteristics of LB pouch cell are shown in Figure 22. A significant reduction in bending stiffness and ultimate bending force at higher temperature was found, but the threshold displacement was not much affected. Slight increases of peak bending, i.e., ultimate force were found at higher loading speed. Simulation results correlate quite well with the test results for all test parameters. To simulate effects of temperature and loading speed, relevant mechanical properties of pouch cell components obtained in tension coupon tests were applied.

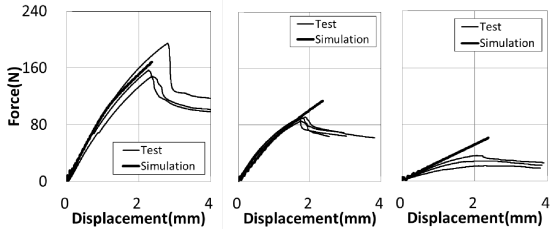

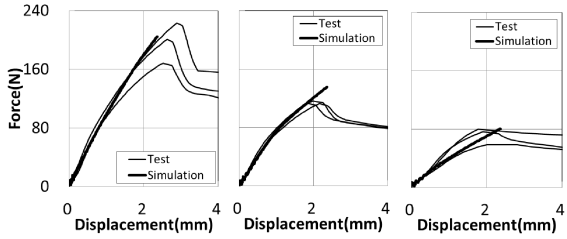

Figure 22. Comparison of test and simulation results of three-point bending test: effects of loading speed and temperature: top 3 graphs, -40 °C (left) 22 °C (middle) 65 °C (right) at 1 mm/min and bottom 3 graphs, -40 °C (left), 22 °C (middle), 65 °C (right) at 490 mm/min.

Impact Hammer and shaker simulations

The same FE model used for the three-point bending simulation was also employed for the impact hammer simulation to analyze modal frequencies of the LB pouch cell. Same impact loading and output acceleration measurement conditions used for the test were applied in the simulation as shown in Figure 23. The resonant frequencies for acceleration amplitude in frequency domain correlate well with the test measurement as listed in Table 4.

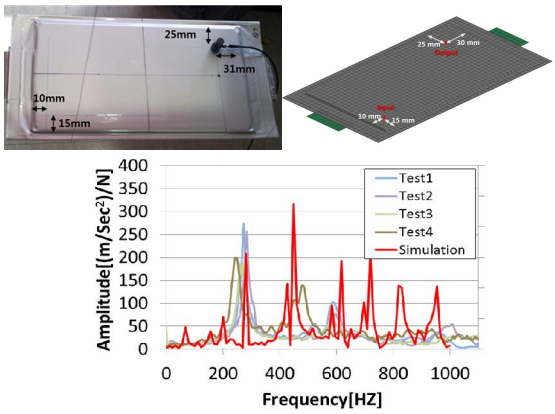

Figure 23. Impact hammer test and simulation setup and result

Table 4 Comparison of natural frequencies from impact hammer test and simulation

Mode	Natural frequency[Hz]		Error [%]
	Simulation	Test	
1st	281	267	5.2
2nd	449	474	5.3
3rd	618	595	3.9

A more practical vibration response of pouch cell was simulated taking the clamping boundary condition into account. A white noise as shown in Figure 24 was created for a sine sweep input signal with frequecy range of 10-2000Hz and 1G amplitude which were same as the test condition. Since acceleration input cannot vibrate the object but only bring a rigid body motion in an explicit analysis, it

was needed to convert the white noise acceleration profile to the velocity input as in Fig. 26.

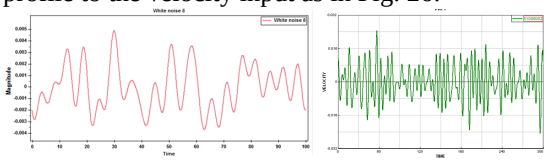

Figure 24. White noise input signal used in shaker vibration simulation; Acceleration profile (left) and converted velocity profile (right)

Figure 25 shows compared vibration responses of pouch cell between test and simluation of shaker escitation. As discussed in the previous section, only vertical excitation with two-edge clamping boundary condition resulted in the natural frequency within the range of durability concern which was 87 Hz, the first mode frequency. Therefore the simulation was focussed on the same boundary and loading conditions. The simulated first two natural frequencies corrleated well with the test measurement as list in Table 5.

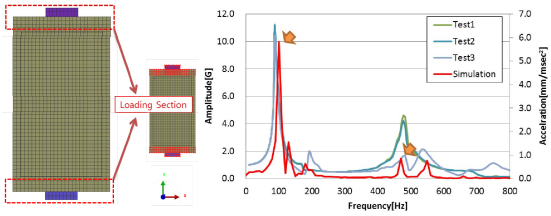

Figure 25. Two-edge clamping boundary condition (left) and acceleration response in frequency domain to the vertical direction excitation (right).

Table 5 Comparison of natural frequencies from shaker excitation test and simulation

Mode	Natural frequency[Hz]		Error [%]
	Simulation	Test	
1st	100	87	12.7%
2nd	470	478	1.7%

DISCUSSION AND LIMITATIONS

Tension coupon test

Since used LB pouch cells with no available information on the number of charge and discharge cycles were employed as test specimen in this study, it was speculated that some degree of mechanical degradation might have occurred at both component and cell levels due to the thermal cyclic loading. Extend of degradation would be unevenly distributed likewise the temperature distribution. Therefore the coupon specimen was consistently extracted at the center portion of the disassembled single layer sheets of separator and electrode to avoid the possible effect of regional degradation differences. The repeatability of electrode was not so good, especially at the higher strain rate and at the lower temperature test conditions. The identification of yield point from stress-strain curve of cathode became a bit obscure due to the short elastic strain region. And the fracture strain of cathode was unusually higher at low temperature than at room and high temperatures. Both electrodes did not show any anisotropy. It was not clear to judge the effects of temperature and strain rate on elastic properties of separator due to the lacking repeatability. Fracture strength and strain of separator were certainly showed their dependencies on temperature, strain rate, and loading direction (i.e., anisotropy); Fracture strength of separator decreased with temperature (i.e., -40℃>22℃>65℃), increased with strain rate (490mm/min>1mm/min), and decreased from transverse to longitudinal direction of the cell (90˚>45˚>0˚). The effects of temperature, strain rate, and loading direction on fracture strain of the separator were precisely opposite to those on fracture strength. Pouch cover showed a similar trend as separator for temperature and strain effects but showed an isotropic behavior.

Impact hammer and shaker excitation tests

Among the four pouch cell specimens for the impact hammer test, 2nd modal frequency was detected from only one pouch cell (specimen #4 in Table 2) but the following 3rd mode, on the other hand, was found alone with the other three pouch cells (specimen #1-3 in Table). This result might come from the impact hammer test condition and the feature of pouch cell used in this study. It was speculated that the accelerometer sensor was placed by chance at one of 2nd mode's nodal positions where the detection of corresponding mode became quite difficult. However, the pouch cell specimen #4 might have different nodal position of the 2nd mode due to the variation of vibration characteristics made in fabrication process. A more refined outcome might be obtained when adopting miniature impact hammer and accelerometer system to analyze the modal shape together with the frequency. Since LB pouch cell has inhomogeneous and nonlinear vibration characteristics, a supplementary shaker excitation test was performed to investigate its further vibration characteristics with more stable loading and boundary conditions. The first natural frequency measured at shaker test, 87Hz with two-edge clamping condition along the out of plane excitation was far lower than the first mode from the impact hammer test (265Hz) and fell within the range of durability concern. Therefore the resonant issue to vehicle level vibration would be with the assembled battery module or pack rather than the design of single detached LB pouch cell.

Finite element modeling of LB pouch cell

Because of thin characteristics of solid-state electrolyte evenly spaced between separator and electrodes layers, each layer of electrolyte was modeled by a link element that connected nodal

points of adjoining elements by a penalty spring with normal and shear stiffness. A force-displacement relation from a three-point bending test for depouched separator/electrode assembly was used to calibrate those normal and shear stiffness of penalty spring in the electrolyte link element. However, a four-point bending could have been a more effective test for separate calibration of normal and shear terms since four-point bending contains a pure bending region where no cross sectional shear stress and strain exist. At first the modeling of pouching vacuum was attempted by applying an external pressure on the pouch cell cover but no good correlations were obtained against test results. It was quite difficult to gauge the degree of vacuum from a completed pouch cell product. And the vacuum for a used cell would not be same as in the initial state due to the internal gas formed during charge and discharge cycles during the service. Therefore the both top and bottom sides of pouch cover was rigidly tied together to model the tight adherence between pouch cover and internal component developed by a pouching vacuum. This modeling was well validated against the three-point bending test result of the pouch cell with and without pouching vacuum. However the tied option cannot properly represent the rigidity change of pouch cell with the degree of the pouching vacuum that is a critical drawback of this approach. The virtual simulation of impact hammer and shaker excitation tests using the finite element model of pouch cell was aimed to predict just natural frequencies. It is expected to extend the simulation to corresponding amplitudes by including damping ratios of each component of pouch cell, which is our future plan.

CONCLUSION

Mechanical characteristics of Lithium-Polymer battery pouch cell were investigated. Tension tests with coupon specimen were performed to measure elastic modulus, yield strength, fracture strength and strains of electrodes, separator, and pouch cover. Effects of temperature, strain rate, and loading direction were also examined. Three-point bending tests on depouched and pouched cells with and without pouching vacuum were conducted to assess stiffness and ultimate strength together with effects of pouching vacuum on its rigidity. Quasi-static and dynamic pin penetration tests were carried out to quantify threshold failure forces of each component and pouch cell, respectively. Vibration characteristics of pouch cell were identified with impact hammer and shaker excitation tests. A virtual simulation model with finite elements is also constructed and validated against test results. A module and pack level tests and computer simulations are scheduled as a following step. Based on this information, further enhancement on the mechanical integrity of pouch cell design will be attempted.

REFERENCES

[1] Elham Sahraei, Rich Hill, Tomasz Wierzbicki, Calibration and finite element simulation of pouch lithium-ion batteries for mechanical integrity, 201, 307– 321, Journal of Power Sources, 2011

[2] Ping Liu, Elena Sherman, Alan Jacobsen, “Design and Fabrication of Multifunctional Structural Batteries”, 646~650, Journal of Power of Sources, 2008

[3] Stephanie Golmon, Kurt Maute, Martin L. Dunn, “Numerical modeling of electrochemical-mechanical interactions in lithium polymer batteries”, 1567~1579, Computers and Structures, 2009

[4] Pam Visual Performance Solution Solver Reference Manual, ESI Group, 2012